InGaAs / AlAsSb quantum cascade lasers

D. G. Revin, L. R. Wilson, E. A. Zibik, R. P. Green, J. W. Cockburn, M. J. Steer, R. J. Airey, and M. Hopkinson

Citation: Appl. Phys. Lett. **85**, 3992 (2004);
View online: https://doi.org/10.1063/1.1814798
View Table of Contents: http://aip.scitation.org/toc/apl/85/18
Published by the American Institute of Physics

InGaAs/AlAsSb quantum cascade lasers

D. G. Revin,[a] L. R. Wilson, E. A. Zibik, R. P. Green, and J. W. Cockburn[b]
Department of Physics and Astronomy, University of Sheffield, Sheffield, S3 7RH United Kingdom

M. J. Steer, R. J. Airey, and M. Hopkinson
EPSRC National Centre for III-V Technologies, Department of Electronic and Electrical Engineering, University of Sheffield, Sheffield, S1 3JD United Kingdom

(Received 26 July 2004; accepted 5 September 2004)

The $In_{0.53}Ga_{0.47}As/AlAs_{0.56}Sb_{0.44}$ heterostructure system is of significant interest for the development of high-performance intersubband devices due to its very large conduction band offset ($\Delta E_c \sim 1.6$ eV) and lattice-matched compatibility with well-established InP-based waveguide technology. In this letter, we report the realization of $In_{0.53}Ga_{0.47}As/AlAs_{0.56}Sb_{0.44}$ quantum cascade lasers emitting at $\lambda \sim 4.3$ μm. The highest-performance devices have low-temperature (20 K) threshold currents of ~ 6 kA/cm^2 and display laser action up to a maximum temperature of 240 K, with a characteristic temperature of $T_0 \sim 150$ K. © *2004 American Institute of Physics*.
[DOI: 10.1063/1.1814798]

As quantum cascade lasers (QCLs) emitting at wavelengths beyond 5 μm approach some degree of technological maturity,[1] attention is turning to seeking similar levels of performance in the technologically important $\lambda \sim 3-5$ μm atmospheric window region. The ultimate limit on short wavelength QCL operation is set by the depth of the quantum wells in the laser active region, i.e., the conduction band offset (ΔE_c) of the heterostructure materials system used. Although strain-compensated InGaAs/AlInAs/InP ($\Delta E_c < \sim 700$ meV) QCLs have been demonstrated at wavelengths down to 3.6 μm (Ref. 2) the performance of such devices is generally inferior to that of longer wavelength QCLs. Consequently, there is strong motivation to extend the QCL concept to materials systems with the highest possible ΔE_c, such as InAs–AlSb (Ref. 3) ($\Delta E_c \sim 2.1$ eV) and $In_{0.53}Ga_{0.47}As-AlAs_{0.56}Sb_{0.44}$ (Ref. 4) ($\Delta E_c \sim 1.6$ eV). However, due to the very high complexity of QCL design, and the stringent demands placed on layer thickness control and uniformity, extension to these materials systems presents considerable challenges.

Recently, we demonstrated intersubband spontaneous emission in the wavelength range 4.1 μm $< \lambda <$ 5.3 μm from quantum cascade structures based on $In_{0.53}Ga_{0.47}As-AlAs_{0.56}Sb_{0.44}$.[5] This heterostructure system, which is lattice matched to InP, is very promising for high-performance QCL development, since it provides a very large ΔE_c as well as complete compatibility with well-established InP-based QCL waveguide design and fabrication technology. In this letter, we report the realisation of $In_{0.53}Ga_{0.47}As-AlAs_{0.56}Sb_{0.44}$ QCLs. Laser emission is observed in pulsed regime at wavelengths of around 4.3 μm up to a maximum temperature of ~ 240 K. Laser performance is found to be strongly dependent upon the thickness of the $AlAs_{0.56}Sb_{0.44}$ injection and exit barriers of the active region.

Three similar QCL designs were studied, each with 30 periods of active and bridging regions consisting of $In_{0.53}Ga_{0.47}As$ quantum wells and $AlAs_{0.56}Sb_{0.44}$ barriers. The designs were based on that of the $\lambda \sim 4.1$ μm quantum cascade structure described in Ref. 5. The major difference in the samples described here is an increase of the bridging region doping density from $\sim 2.5 \times 10^{17}$ cm^{-3} to $\sim 8 \times 10^{17}$ cm^{-3}. This allows the devices to sustain higher currents than those reported in Ref. 5, allowing lasing thresholds to be reached. In addition, by varying the thickness of the injection and exit barriers of the active region and monitoring the effects on laser characteristics we have improved the electron injection and extraction efficiencies of the active region, which are mainly controlled by these barriers. Such empirical optimization is essential for devices in this materials system, due to uncertainties arising from compositional grading at the interfaces and the fact that values of certain key parameters such as $AlAs_{0.56}Sb_{0.44}$ electron effective mass and conduction band offset are not yet precisely known.

The layer thicknesses (in angstroms) for one period of active and bridging regions for the three QCL samples studied were as follows: **W1**/18/**9**/46/**9**/42/**W2**/32/**13**/30/**13**/<u>30</u>/**14**/<u>28</u>/**14**/<u>26</u>/**14**/<u>24</u>/**15**/<u>22</u>/**15**/21. The $AlAs_{0.56}Sb_{0.44}$ layers (barriers) are in bold font, the InGaAs wells are in Roman font, and the underlined layers are Si-doped to $n = 8 \times 10^{17}$ cm^{-3}. The various values of W1 (injection barrier width) and W2 (exit barrier width) for the three QCL designs are given in Table I. A section of the calculated conduction band profile and active region electron wave functions for sample 2060 are shown in Fig. 1. The energy levels, wave functions, and dipole matrix elements were calculated by solving the Schrödinger equation using a one band model with an energy dependent effective mass. The material parameters used in the Schrödinger simulations are $\Delta E_c = 1.6$ eV, electron effective masses $m^* = 0.042 m_0$ for $In_{0.53}Ga_{0.47}As$ and $m^* = 0.125 m_0$ for $AlAs_{0.56}Sb_{0.44}$, and nonparabolicity coefficient for $In_{0.53}Ga_{0.47}As$, $\gamma = 1.13 \times 10^{-18}$ m^{-2}.

The samples were grown on n^+-InP (100) substrates by molecular beam epitaxy using As_2 and Sb_2 group V species with valved cracker sources. Growth interruption was employed at every interface while maintaining continuous As flux to minimize fluctuations in composition across the heterointerfaces. Prior to growth of the QCL structures growth

[a]Permanent address: Institute for Physics of Microstructures, Russian Academy of Science, 603950 Nizhny Novgorod, Russia.
[b]Electronic mail: j.cockburn@sheffield.ac.uk

TABLE I. Summary of design parameters and characteristics of QCLs studied.

Sample No.	Injection barrier width (W1) (nm)	Exit barrier width (W2) (nm)	Threshold ($T=20$ K) current density (kA/cm^2)	Wavelength of laser emission (calculated wavelength) (μm)
2059	2.1	1.7	9.3	4.3 (4.05)
2060	2.1	1.1	5.9	4.36 (4.2)
2061	2.7	1.4	22	4.35(4.18)

calibrations were made on the test superlattice structures with similar barrier-well thickness in order to ensure good lattice matching of all layers to the InP substrate. Full details of the growth process can be found in Ref. 5.

The QCL wafers were processed by wet etching into laser ridge structures 20 μm wide and 1.5 mm long and soldered epilayer-up to copper submounts without any facet coatings. Nonalloyed Ti/Au top and bottom contacts were used. Waveguide losses of around 5 cm^{-1} were measured for the processed ridges by means of a Fabry–Pérot resonator technique[6] employing a commercial single mode $\lambda \sim 5.3$ μm QCL (Alpes Laser) as the probe source. For characterization of intersubband emission, the samples were mounted onto the cold finger of a continuous flow helium cryostat and driven at 10 kHz with 1 μs long current pulses to measure spontaneous emission and 100 ns pulses for laser operation.

Devices from all three wafers displayed laser emission at wavelengths close to the predicted values (Table I). This good agreement confirms the reproducibility and reliability of the growth process and provides confidence in the materials parameters used in the device design. As shown in Table I, significant differences were observed in the threshold current densities of the three samples, with the value for sample 2060 being much lower than that for either samples 2059 or 2061. Moreover no laser emission was observed for the 2059 and 2061 samples at temperatures higher than 140 K. This shows how sensitively device performance depends on injection and exit barrier thicknesses. A narrow exit barrier helps to extract electrons from the low levels of the active region into the bridging region. The thickness of the exit barrier (1.1 nm) for sample 2060 makes it comparable with the thickness of the other barriers in the bridging region. Thus, in this case the active region spans the whole period and the design of this sample becomes similar to a "bound-to-continuum" design,[7] where the emission occurs between a state localized close to the injection barrier and a miniband of the "active region." It has been shown[7] that this design produces better electron extraction efficiency from the low-lying energy levels that are closest to the exit barrier. Our results also suggest that the thickness of the injection barrier (which controls the splitting energy between upper level in the active region and lower level in bridging region) should be less than about 2 nm in order to provide efficient injection of electrons and maintain the intersubband population inversion over a relatively wide range of applied voltage. Increasing this barrier width from 2.1 to 2.7 nm results in a dramatic decrease of this splitting energy from 2.8 meV to less than 1 meV making the tunneling probability into the upper level of the active region much smaller. Further gradual reduction of the injection barrier width seems to be an appropriate change of the design for further improvement of laser performance.[8]

The electroluminescence and laser spectra for the 2060 sample measured at temperatures of 20 and 240 K (the maximum temperature for laser emission for this sample) are shown in Fig. 2. The spectra were measured with a Fourier-transform spectrometer and liquid nitrogen-cooled mercury cadmium telluride (MCT) detector using step scan and lock-in detection techniques. Current-dependent full widths at half maximum from 19 to 3 meV were measured for spontaneous emission spectra for current densities below the threshold. As temperature increases from 20 to 240 K the laser emission energy shifts down by 9 meV while its optical intensity decreases by a factor of 100. This temperature limitation is thought to mainly originate from thermal backfilling of the lower laser levels in the active region by hot electrons from the bridging region, which reduces the population inversion. It is likely that increasing the energy width (about 80 meV) of the miniband in the bridging region either by incorporating additional well-barrier pairs or modifying the design for higher applied voltage could help to improve the high temperature performance.

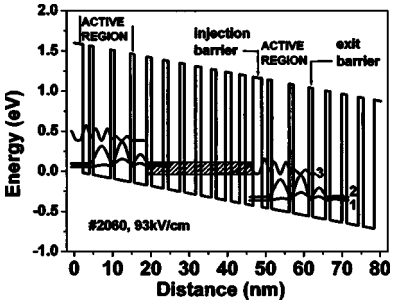

FIG. 1. Conduction band profile for sample 2060 under applied electric fields of 93 kV/cm. The moduli squared of the relevant wave functions in the active region are labeled 1, 2, and 3. The laser transition occurs from level 3 to level 2. The lowest miniband in the injector region (schematically shown by grey box) extracts electrons from the lowest levels (1 and 2) in the active regions and injects them into the highest level (3) in the next active region.

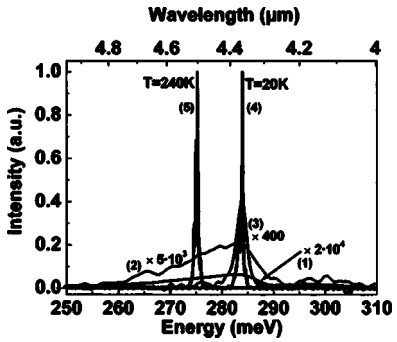

FIG. 2. Low temperature ($T=20$ K) spontaneous emission and laser spectra for sample 2060. Current density kA/cm^2: (1) −3.7, (2) −4.7, (3) −5.8, (4) −6.2. High-temperature ($T=240$ K) laser spectrum (5) taken at 16.2 kA/cm^2.

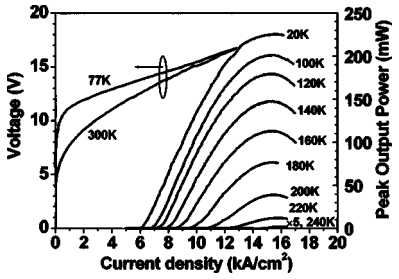

FIG. 3. Voltage and peak light power vs current characteristics of the sample 2060 at various heat sink temperatures.

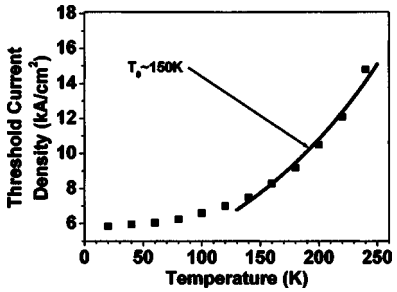

FIG. 4. Threshold current density as a function of temperature for sample 2060. The solid line shows an exponential fit of data over the 140–240 K range which gives a characteristic temperature $T_0 = 150$ K.

In Fig. 3 the voltage versus current and peak light output power versus current characteristics of the 2060 sample at different temperatures are plotted. It should be stressed that electrical characteristics of all three samples are very robust and they can easily sustain current densities of more than 20 kA/cm^2 without any degradation. Laser peak powers of up to 230 mW were detected at 20 K. The light was collected with approximately 50% efficiency from only one facet of the laser ridge and measured with a calibrated MCT detector. The threshold current density at 20 K is measured to be 5.9 kA/cm^2 and increases up to about 15 kA/cm at 240 K. The characteristic temperature (T_0) value for $I_{\mathrm{th}} = I_{\mathrm{th}}(0)\exp(T/T_0)$ dependence defined between 140 and 240 K is found to be approximately 150 K (see Fig. 4). The factor of 2.5 increase in the threshold current density as the temperature is raised from 20 to 240 K is very similar to that observed for $\lambda \approx 5$ μm InGaAs/AlInAs QCLs in which the temperature dependence was shown to be solely due to the increasing phonon population with temperature.[9] This suggests that thermally activated carrier leakage has a negligible effect on threshold current densities in these structures.

In conclusion, we have demonstrated InP-based quantum cascade lasers containing $In_{0.53}Ga_{0.47}As-AlAs_{0.56}Sb_{0.44}$ core regions. Three samples with different injection and exit barriers have been studied, all exhibiting very stable electrical and optical characteristics. Peak optical laser powers of several hundreds of milliwatts at 20 K have been detected for the best sample. Laser emission from all samples has been observed very close to the calculated wavelength of $\lambda \sim 4.3\mu$m.

This work is supported by the Engineering and Physical Sciences Research Council (EPSRC) UK Grant No. GR/R25576, by EU FP6 Grant No. STRP 505642 "ANSWER," and the award of an Advanced Fellowship to L.R.W.

[1]See, for example A. Evans, J. S. Yu, J. David, L. Doris, K. Mi, S. Slivken, and M. Razeghi, Appl. Phys. Lett. **84**, 314 (2004).
[2]J. Faist, F. Capasso, C. Sirtori, D. L. Sivco, J. N. Baillargeon, A. L. Hutchinson, S.-N. G. Chu, and A. Y. Cho, Appl. Phys. Lett. **68**, 3681 (1996).
[3]R. Teissier, D. Barate, A. Vicet, D. A. Yarekha, C. Alibert, A. N. Baranov, X. Marcadet, M. Garcia, and C. Sirtori, Electron. Lett. **39**, 1252 (2003).
[4]N. Georgiev and T. Mozume, J. Appl. Phys. **89**, 1064 (2001).
[5]D. G. Revin, L. R. Wilson, E. A. Zibik, R. P. Green, J. W. Cockburn, M. J. Steer, R. J. Airey, and M. Hopkinson, Appl. Phys. Lett. **84**, 1447 (2004).
[6]D. G. Revin, L. R. Wilson, D. A. Carder, J. W. Cockburn, M. J. Steer, M. Hopkinson, R. J. Airey, M. Garcia, C. Sirtori, Y. Rouillard, D. Barate, and A. Vicet, J. Appl. Phys. **95**, 7584 (2004).
[7]J. Faist, M. Beck, T. Aellen, and E. Gini, Appl. Phys. Lett. **78**, 147 (2001).
[8]C. Sirtori, F. Capasso, J. Faist, A. L. Hutchinson, D. L. Sivco, and A. Y. Cho, IEEE J. Quantum Electron. **34**, 1722 (1998).
[9]J. Faist, F. Capasso, C. Sirtori, D. L. Sivco, J. N. Baillargeon, A. L. Hutchinson, S. G. Chu, and A. Y. Cho, Appl. Phys. Lett. **68**, 3680 (1996).